

A Fully Open-source Implementation of an Analog 8-PAM Demapper for High-speed Communications

Mohamed Aiham Hemza*, Alex Alvarado*, Krzysztof Herman[†], Piyush Kaul*

*Eindhoven University of Technology, Eindhoven, the Netherlands

[†]IHP - Leibniz-Institut für innovative Mikroelektronik, Frankfurt (Oder), Germany

Abstract—Spectrally-efficient communication systems rely on the use of multi-level modulation formats. At the receiver side, a demodulator is often used to extract soft information about the transmitted bits. Such a demodulator is typically implemented in the digital domain. However, analog implementations of such demodulators are also possible. In this paper, we design and simulate an analog 8-ary pulse-amplitude modulation (8-PAM) demapper in IHP SG13G2 SiGe BiCMOS technology. We generalize and improve a design available in the literature for 4-PAM. A fully MOSFET-based 8-PAM design is proposed. Our simulations and design are completely based on open-source IC design tools. Our results show an energy efficiency of 0.33 pJ/bit for a data rate of 1 Gbit/s.

Index Terms—BiCMOS, Demapper, Integrated Circuits, Open Source PDKs, Quadrature Amplitude Modulation, SiGe.

I. INTRODUCTION

Modern communication systems rely on spectrally-efficient modulation formats, such as quadrature amplitude modulation (QAM). These formats are combined with forward error correction (FEC) to achieve high data rates. In such systems, the receiver typically provides soft information to the FEC decoder in the form of log-likelihood ratios (LLRs). This architecture is known as bit-interleaved coded modulation [1]–[3].

In conventional receivers, an analog-to-digital converter (ADC) is used to enable LLR computations in the digital domain. These LLRs are then processed by the FEC decoder, which also operates in the digital domain. As data rates continue to grow, the power consumption of digital circuits is rapidly growing, making it increasingly difficult to maintain a low energy per bit. Technology scaling has traditionally reduced power consumption, however, recent scaling trends have limited these gains. These challenges motivate research into receiver frontends that generate LLRs *directly in the analog domain*. The ultimate goal is to improve energy efficiency and speed by adopting architectures that do not rely on ADCs.

Analog FEC decoders received considerable attention in the late 1990’s and early 2000’s [4]–[8]. These works can be traced back to the seminal work of Loeliger and Hagenauer [9], [10] who recognized that the processing required in FEC decoders can be implemented using analog electronics. On the other hand, analog demappers have rarely been studied in the literature. This lack of results is slightly surprising, as analog demappers are arguably essential for implementing a

fully analog receiver, which will be based on a concatenation of an analog demapper and an analog FEC decoder.

The first analog 16-QAM demapper was proposed in [11]. The design in [11] focuses on the constituent 4-PAM constellation and uses a PMOS differential-pair with BJT current-mirror loads to compute *approximated* LLRs. These LLRs are piece-wise linear functions of the channel observation and are obtained when the max-log approximation is used [3, Sec. 3.3.3]. The circuit in [11] was simulated in a 0.25 μm BiCMOS process and relies on a hybrid design combining MOSFETs and BJTs. Two years later, [12] presented an analog circuit that computes the *exact* LLRs by exploiting the exponential current characteristics of MOSFETs in weak inversion. The results in [11], [12] are limited to 4-PAM. Furthermore, no performance metrics (such as demapping speed or energy efficiency) were reported in [11], [12].

In this paper, we revisit the approach of [11] and extend it to realize an 8-PAM analog demapper. Unlike the hybrid implementation in [11], our proposed design is fully based on MOSFETs. This choice is shown to offer improved speed and lower power consumption for the same circuit configuration. The design is implemented using the IHP-Open-PDK [13]¹, which provides the SG13G2 SiGe BiCMOS technology. This process integrates HBTs operating in the sub-terahertz range on top of a fully functional CMOS platform.

II. SYSTEM MODEL AND LLR COMPUTATIONS

We consider communication over the additive white Gaussian noise channel. A typical baseband receiver architecture for such a system includes an ADC followed by different digital signal processing subsystems (e.g., equalization, demapping, and decoding). We consider 8-PAM with equally spaced symbols, thereby effectively considering 64-QAM. The transmitted bits b_1, b_2, b_3 are assumed to be independent and uniformly distributed. The transmitted symbol x is modeled as a discrete random variable, uniformly distributed over the 8-PAM constellation, i.e., $X \sim \mathcal{U}(\mathcal{A})$, where $\mathcal{A} = \{\pm 7d, \pm 5d, \pm 3d, \pm 1d\}$. The scaling factor d is chosen so that the average symbol energy is $\mathbb{E}[X^2] = 0.5$, and thus, the QAM constellation has unit energy. The bit-to-symbol mapping (\mathcal{M}) is based on the binary-reflected Gray code [14].

This work has been partially funded by the Eindhoven Hendrik Casimir Institute (EHCI) Collaborative Projects Program and by FMD-QNC No. 16ME0831 financed by Federal Ministry of Research, Technology and Space. Corresponding author: a.alvarado@tue.nl

¹Recent open-source initiatives by SkyWater, GlobalFoundries and IHP have made chip design and fabrication more accessible, while the associated tools such as Qucs-S, ngspice and OpenVAF, used throughout this work, enable reliable and transparent circuit design within an open-source framework.

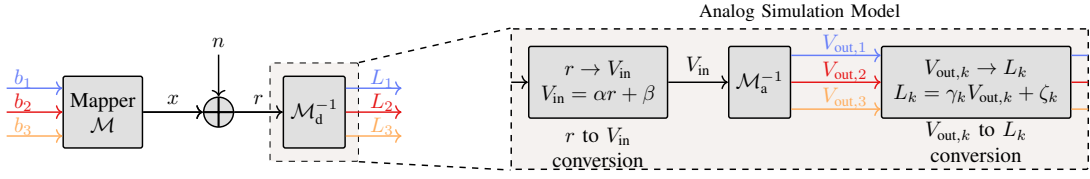


Fig. 1. System model of the considered 8-PAM transmission. Bits b_1, b_2, b_3 are mapped to constellation symbols, transmitted over the channel, and converted into LLRs L_1, L_2, L_3 by the demapper. The r.h.s. of this figure shows the simulation model used for the proposed analog implementation of the demapper.

At every discrete-time instant, the received signal is $r = x + n$, where the noise $N \sim \mathcal{N}(0, \sigma^2)$ is Gaussian. In a traditional receiver, the received signal r represents the digital signal that is fed to a digital demapper \mathcal{M}_d^{-1} , which produces the LLRs L . This configuration is shown in Fig. 1 (left) for the case of 8-PAM, where 3 LLRs are computed for each r .

An LLR gives a soft estimate of how likely a transmitted bit is (1 or 0), given the received symbol [3]. It is defined as

$$L_k \triangleq \log \frac{p_{R|B_k}(r|1)}{p_{R|B_k}(r|0)}, \quad (1)$$

where B_k is the k -th bit in the symbol and $p_{R|B_k}(r|b)$ is the likelihood of receiving r assuming $B_k = b$. For the channel under consideration, the LLR in (1) is

$$L_k = \log \sum_{i \in \mathcal{I}_k^1} e^{-\frac{(r-x_i)^2}{2\sigma^2}} - \log \sum_{i \in \mathcal{I}_k^0} e^{-\frac{(r-x_i)^2}{2\sigma^2}}, \quad (2)$$

where \mathcal{I}_k^b is the set of indices of constellation points where bit $B_k = b$ and the signal to noise ratio (SNR) is $\text{SNR} \triangleq 1/2\sigma^2$.

The exponential functions in (2) decay rapidly, and thus, the terms in the LLR expression are dominated by the smallest distances $(r - x_i)^2$. Therefore, an approximation is obtained by retaining only the x_i closest to r from \mathcal{I}_k^b . This leads to the max-log approximation [3, eq. (3.99)]

$$L_k \approx \text{SNR} \left(\min_{i \in \mathcal{I}_k^0} (r - x_i)^2 - \min_{i \in \mathcal{I}_k^1} (r - x_i)^2 \right). \quad (3)$$

Fig. 2 shows the exact and max-log LLRs with black and green lines, resp. The x-axis shown is scaled and shifted to map the constellation points \mathcal{A} to the analog demapper's input range. Details on this scaling and shifting are given in Sec. III. The results in this figure show how the max-log approximation effectively converts the nonlinear relationship between r and L_k (black lines) into a piece-wise linear function (green lines). This figure also shows results obtained using analog circuits (red and blue lines), whose design is discussed next.

III. PROPOSED DESIGN

Here we consider using an analog demapper \mathcal{M}_a^{-1} to replace the digital demapper \mathcal{M}_d^{-1} in Fig. 1. This analog demapper is fully described by its input-output relationship, where V_{in} is the input voltage, and $V_{\text{out},k}$ with $k = 1, 2, 3$ are the output voltages. To implement such an analog demapper, [11] proposed using a cell-based approach, where each cell generates a piece-wise linear function. These cells are then combined to obtain the piece-wise linear relationship created

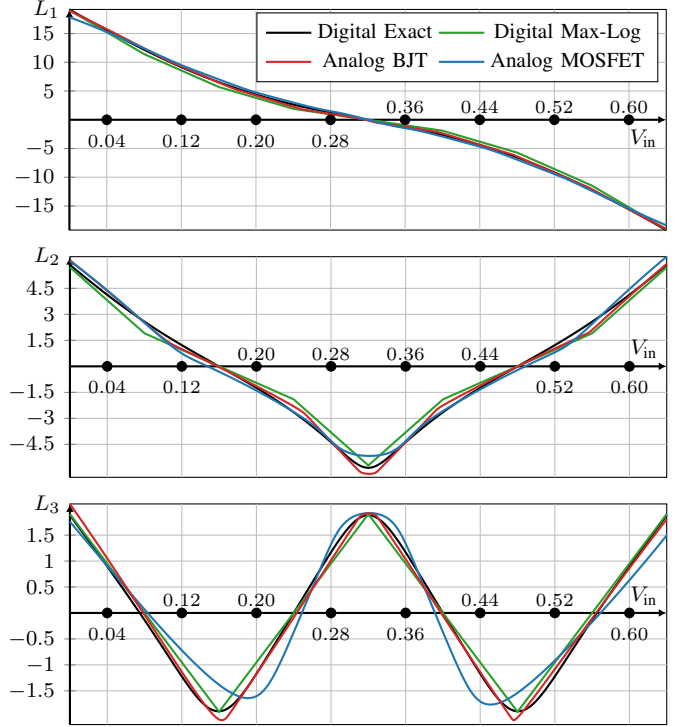


Fig. 2. LLRs for bit positions $k = 1$ (top), $k = 2$ (middle), and $k = 3$ (bottom) at SNR = 10 dB. The received symbol r is scaled by (α, β) to obtain V_{in} . The scaled constellation points are also shown. The analog demapper output voltages V_{out} are scaled by (γ_k, ζ_k) to obtain the LLRs.

by the max-log approximation in (3). The cell proposed in [11] is shown in Fig. 3. The resulting single piece-wise function is shown with a red line in the inset of Fig. 3.

The cell in Fig. 3 operates as a current-steering stage that converts V_{in} into a piece-wise linear output current. Transistors $P3$ - $P4$ generate a bias current I_{bias} which is mirrored into the PMOS differential pair $P1$ - $P2$. Depending on the values of V_{in} and V_{ref} , more current is directed toward I_1 or I_2 , modulating the collector currents of $Q1$ - $Q2$. $Q1$ - $Q2$ mirror the current I_1 to I_3 depending on the relation between I_1 and I_2 . By Kirchhoff's current law, $I_4 = I_2 - I_3$ which is then mirrored by $Q3$ - $Q4$ translating it to I_{out} . BJTs were proposed in [11] to be used in the mirrors for improved linearity, effectively trying to mimic the max-log approximation in the best possible way. The voltage transfer characteristic can be analyzed based on three cases for V_{in} and V_{ref} :

Case 1 ($V_{\text{in}} < V_{\text{ref}}$): $P2$ sinks more current than $P1$, so $I_2 > I_1$. $I_1 = I_3$ and $I_{\text{out}} = I_2 - I_1$, giving $V_{\text{out}} = V_{\text{DD}} - I_{\text{out}}R_{\text{out}}$.

Case 2 ($V_{\text{in}} = V_{\text{ref}}$): $P1$ - $P2$ conduct equal current $I_2 = I_1$,

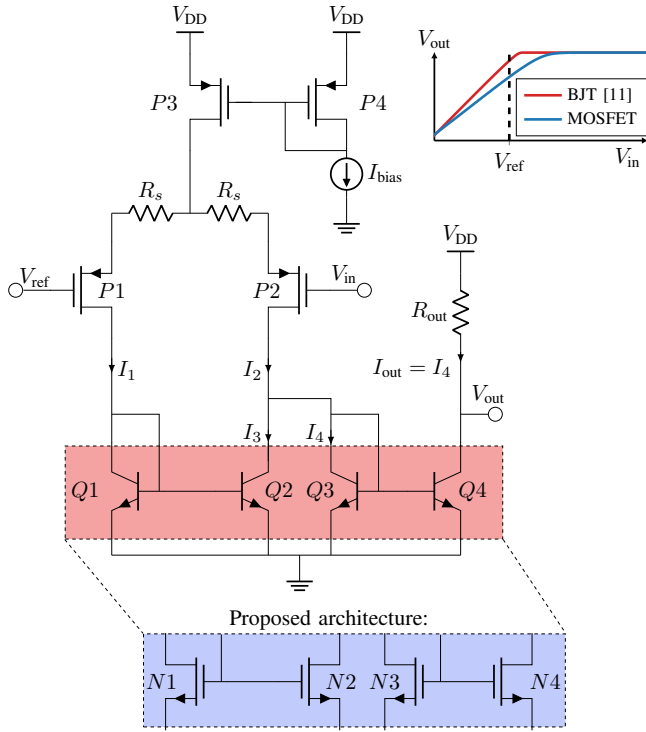


Fig. 3. Single cell implementing one segment of the piece-wise linear LLR function. The inset shows the transfer characteristics for the original design [11] (BJTs) and our proposed architecture (MOSFETs).

therefore, $I_{out} = 0$ and $V_{out} = V_{DD}$.

Case 3 ($V_{in} > V_{ref}$): $P2$ sinks less current than $P1$. As a result, $Q2$ is driven into saturation (base-emitter and base-collector are forward biased). No current is mirrored through $Q1$ - $Q2$, hence $I_3 = I_2$. Therefore $I_{out} = 0$ and $V_{out} = V_{DD}$.

The voltage transfer function in the inset of Fig. 3 shows a positive slope, followed by constant voltage $V_{out} = V_{DD}$. Swapping V_{in} and V_{ref} generates a constant voltage $V_{out} = V_{DD}$ followed by a descending slope. The 8-PAM LLRs are then realized by adding and subtracting the output currents of multiple cells with different reference voltages. To allow this, a differential output structure is employed, where each cell contributes either to the positive or the negative output branch, resulting in

$$V_{out} = V_{DD} - \left(\sum_{i \in \text{pos}} I_{out,i} - \sum_{i \in \text{neg}} I_{out,i} \right) \cdot R_{out}, \quad (4)$$

where $i \in \text{pos}$ ($i \in \text{neg}$) corresponds to cells whose output currents contribute positively (negatively) to the output.

While the cell proposed in [11] provides good linearity, its operation speed is limited by charge storage effects when the BJTs enter saturation. To overcome this limitation, we propose to replace $Q1$ - $Q4$ with NMOS transistors $N1$ - $N4$. This slightly reduced the linearity of the piecewise characteristic, as shown in the inset of Fig. 3. However, as we will see in Sec. IV, using NMOS enables higher operating speed and lower energy consumption. In the following sections, the circuit from [11] and the newly proposed design are referred to as the BJT and MOSFET designs, respectively.

To ensure that $P1$ - $P4$ remain in saturation², the input voltage was limited to $V_{in} \leq 0.64$ V. The supply voltage was fixed to the maximum allowed by the technology, i.e., $V_{DD} = 1.6$ V. The output resistance was set to $R_{out} = 3$ k Ω . This value can be optimized depending on the subsequent stage. The source resistance $R_s = 500$ Ω helps maintain output linearity over a wide range of input voltage swings. The transistors were left at minimum size (0.15 μm width and 0.14 μm length for MOSFETs and 1 emitter with length 0.9 μm for BJTs).

IV. RESULTS AND DISCUSSION

To simulate the analog demapper, the input is a voltage V_{in} rather than r , and the outputs $V_{out,k}$ are voltages rather than a digital LLRs. To enable a fair comparison, conversion blocks are introduced, as shown in Fig. 1. The input voltage is mapped via $V_{in} = \alpha r + \beta$, where (α, β) define the mapping between the constellation points \mathcal{A} and the circuit's input range. They were chosen such that $r = -7d$ and $r = +7d$ map to $V_{in} = 0.04$ V and $V_{in} = 0.60$ V respectively, resulting in $\alpha = 0.2592$ and $\beta = 0.32$. The analog outputs are then linearly transformed per bit as $L_k = \gamma_k V_{out,k} + \zeta_k$, where (γ_k, ζ_k) are obtained by minimizing the squared amplitude error with respect to the reference LLRs, i.e.,

$$(\gamma_k, \zeta_k) = \underset{\gamma, \zeta}{\text{argmin}} \int_{-\infty}^{\infty} (\gamma V_{out,k}(r) + \zeta - L_k(r))^2 dr, \quad (5)$$

where L_k is given by (2) and the dependency of L_k and $V_{out,k}$ on the channel observation r was made explicit. The optimization (5) is performed for each SNR.

The performance of the analog demapper is evaluated by considering an information-theoretic metric called achievable rate [15]. An achievable rate per bit position is the so-called bit-wise mutual information (MI) $I(B_k; L_k)$. Let $B_k \in \{0, 1\}$ denote the random bit in position k and L_k its LLR. The MI between B_k and L_k can be approximated via [3, eq. (4.82)]

$$I(B_k; L_k) \approx 1 - \mathbb{E}[\log_2(1 + \exp((-1)^{B_k} L_k))], \quad (6)$$

where $\mathbb{E}[\cdot]$ represents expectation. An achievable rate for the system under consideration with 8-PAM is the average bit-wise MIs, often referred to as the generalized mutual information (GMI) and is expressed as

$$\text{GMI} = \frac{1}{3} \sum_{k=1}^3 I(B_k; L_k). \quad (7)$$

In what follows, we will also present results in terms of the rate penalty caused by the approximations. This penalty is defined as the loss caused by max-log or the two analog demappers, in terms of GMI, with respect to the GMI obtained when using exact LLRs. Lastly, bit error rate (BER) is presented by performing hard decisions on the LLRs: $b_k = 1$ if $L_k \geq 0$ and $b_k = 0$ if $L_k < 0$.

²Note that MOSFET saturation occurs when the channel is pinched off near the drain, and is different than BJT saturation.

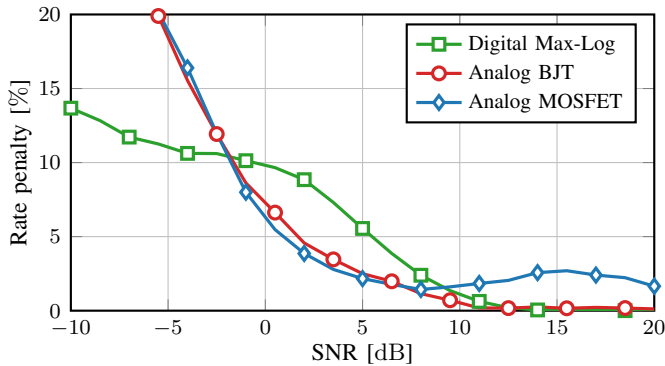


Fig. 4. Rate penalty relative to the digital exact demapper vs SNR of the max-log, BJT and MOSFET approximations

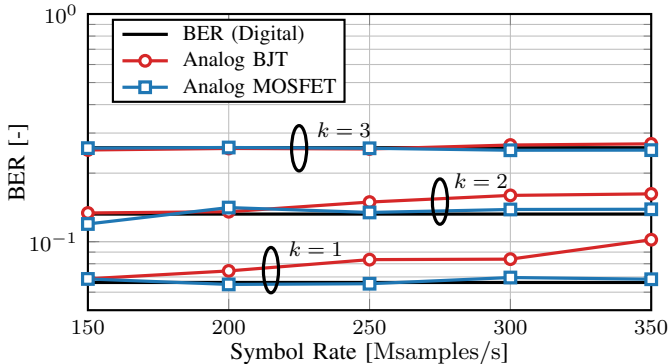


Fig. 5. BER performance over sampling frequency. The horizontal lines indicate the reference BER from hard decisions on LLRs from the digital exact demapper at SNR = 10 dB, representing the best achievable performance.

A DC sweep of the input voltage was used to obtain the transfer characteristic and corresponding LLRs. Fig. 2 shows the LLRs for the exact, max-log, BJT, and MOSFET approximations, indicating that the analog results closely follow the digital references for $k = 1$ and $k = 2$. For $k = 3$ the BJT approximation is still very precise, however, the MOSFET approximation deviates substantially from the exact LLRs.

Monte Carlo simulations were performed to evaluate the GMI. The results are shown in Fig. 4. The max-log and BJT demappers approach 0% penalty at high SNR, while the MOSFET demapper remains within 3% for SNRs above 3 dB due to the deviation of the LLR for bit position $k = 3$ as mentioned earlier. The results in Fig. 4 also show that when $-1 \text{ dB} \leq \text{SNR} \leq 9 \text{ dB}$, the analog demappers outperform the (digital) max-log demapper. These results can be explained by the fact that the first two bit positions ($k = 1, 2$) are the ones that contribute the most to the GMI in (7). As shown in Fig. 2 (top and middle), the analog demappers approximate the exact LLRs better than the max-log approximation for those bit positions.

A transient simulation was performed to evaluate demapping speed. The input of the analog demapper are voltage levels of a sequence of square pulses of varying symbol rate. The output of the analog demapper was sampled, which allowed us to assess the circuit's dynamic response and settling behavior. The resulting BER performance is shown in Fig. 5.

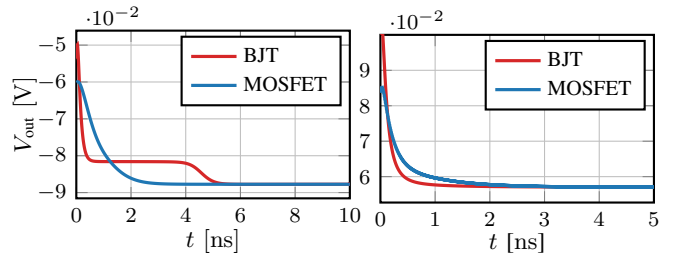


Fig. 6. Comparison of the settling behavior for two symbol transitions in the BJT and MOSFET demappers for $k = 1$: Transition from $r = +3d$ to $r = +7d$ (left) and from $r = -7d$ to $r = -5d$ (right). A vertical offset has been applied to the MOSFET waveforms to allow comparison.

From Fig. 5, it can be seen that the BJT demapper exhibits an increasing BER as the symbol rate rises, while the MOSFET design maintains a constant BER across the entire symbol rate range, very close to that of the ideal (digital) demapper. This behavior can be further understood from Fig. 6 (left), which illustrates the output voltage dynamics for a symbol transition that requires certain cells to be driven out of saturation. As the BJTs exit the saturation region, they must first discharge their base, resulting in the plateau visible in the red waveform. The MOSFET, however, does not show such a plateau, and thus, settles much faster (after $t \approx 2 \text{ ns}$). On the other hand, Fig. 6 (right) corresponds to a transition where all relevant BJT cells are in the forward-active region, therefore no BJT needs to come out of saturation. In this case, no plateau appears in the BJT response, showing that if BJTs remain out of saturation, the demapper based on BJTs can achieve settling behavior comparable to that of the MOSFET circuit.

To obtain the results shown in Fig. 5, the BJT and MOSFET designs were biased at $I_{\text{bias}} = 100 \mu\text{A}$ and $I_{\text{bias}} = 10 \mu\text{A}$ per cell, resp. Reducing the bias current in the BJT design led to a significant increase in BER, and thus, a relatively high bias current had to be used ($I_{\text{bias}} = 100 \mu\text{A}$). Our MOSFET design on the other hand, offers a near-optimum BER performance for symbol rates up to 350 Msamples/s, which corresponds to a bit rate of about 1 Gbit/s. The power consumption of our design is 0.35 mW, i.e., 0.33 pJ/bit at 1 Gbit/s.

V. CONCLUSIONS

This paper presented a fully open-source implementation of an analog 8-PAM demapper. The proposed design achieves an energy efficiency of 0.33 pJ/bit for a data rate of 1 Gbit/s. Compared to digital demappers, the proposed solution provides analog LLRs that can be directly interfaced with an analog FEC decoder. The results highlight a trade-off between accuracy and speed across BJT and MOSFET implementations and confirm the potential of efficient analog demappers for high-speed communication systems.

The results in this paper are simple proof-of-concept results highlighting the capabilities of the open-source design flow based on IHP-Open-PDK and open-source EDA tools. Future research includes an analysis of analog demappers for denser, geometrically-shaped constellations. Future work also includes PVT simulations and an analysis of the impact of circuit noise on the design.

REFERENCES

- [1] E. Zehavi, "8-PSK trellis codes for a Rayleigh channel," *IEEE Trans. Inf. Theory*, vol. 40, no. 5, pp. 873–884, May 1992.
- [2] G. Caire, G. Taricco, and E. Biglieri, "Bit-interleaved coded modulation," *IEEE Trans. Inf. Theory*, vol. 44, no. 3, pp. 927–946, May 1998.
- [3] L. Szczecinski and A. Alvarado, *Bit-Interleaved Coded Modulation: Fundamentals, Analysis and Design*. Chichester, UK: John Wiley & Sons, 2015.
- [4] F. Lustenberger, M. Helfenstein, H.-A. Loeliger, F. Tarkoy, and G. Moschytz, "An analog VLSI decoding technique for digital codes," in *Proc. IEEE International Symposium on Circuits and Systems (ISCAS)*, Orlando, FL, May/June 1999.
- [5] M. Moerz, T. Gabara, R. Yan, and J. Hagenauer, "An analog 0.25 μm BiCMOS tailbiting MAP decoder," in *Proc. IEEE International Solid-State Circuits Conference (ISSCC)*, San Francisco, CA, Feb. 2000.
- [6] A. Xotta, D. Vogrig, A. Gerosa, A. Neviani, A. Graell i Amat, G. Montorsi, M. Bruccoleri, and G. Betti, "An all-analog CMOS implementation of a turbo decoder for hard-disk drive read channels," in *2002 IEEE International Symposium on Circuits and Systems (ISCAS)*, Phoenix-Scottsdale, AZ, May 2002.
- [7] S. Hemati and A. Banihashemi, "Dynamics and performance analysis of analog iterative decoding for low-density parity-check (LDPC) codes," *IEEE Trans. Commun.*, vol. 54, no. 1, pp. 61–70, 2006.
- [8] M. Mörz, "Analog signal processing in forward error correction (FEC) decoders," Ph.D. Dissertation, Technische Universität München, Munich, Germany, 2007.
- [9] J. Hagenauer, E. Offer, C. Méasson, and M. Mörz, "Decoding and equalization with analog non-linear networks," *AEU Int. J. Electron. Commun.*, vol. 51, no. 1, pp. 2–12, Jan. 1997.
- [10] H.-A. Loeliger, F. Lustenberger, M. Helfenstein, and F. Tarkiy, "Probability propagation and decoding in analog VLSI," *IEEE Trans. Inf. Theory*, vol. 47, no. 2, pp. 837–843, Feb. 2001.
- [11] F. Seguin, C. Lahuec, J. Lebert, M. Arzel, and M. Jezequel, "Analogue 16-QAM demodulator," *Electronics Letters*, vol. 40, pp. 1138–1140, Sep. 2004.
- [12] M. Frey, H.-A. Loeliger, and P. Merkli, "Analog circuits for symbol-likelihood computation," in *Proc. International Conference on Electronics Circuits and Systems (ICECS)*, Nice, France, Dec. 2006.
- [13] K. Herman, N. Herfurth, T. Henkes, S. Andreev, R. Scholz, M. Müller, M. Krattenmacher, H. Pretl, and W. Grabinski, "On the versatility of the IHP BiCMOS open source and manufacturable PDK: A step towards the future where anybody can design and build a chip," *IEEE Solid-State Circuits Magazine*, vol. 16, no. 2, pp. 30–38, 2024.
- [14] E. Agrell, J. Lassing, E. G. Ström, and T. Ottosson, "On the optimality of the binary reflected Gray code," *IEEE Trans. Inf. Theory*, vol. 50, no. 12, pp. 3170–3182, Dec. 2004.
- [15] C. E. Shannon, "A mathematical theory of communications," *Bell System Technical Journal*, vol. 27, pp. 379–423 and 623–656, July and Oct. 1948.